PHYSICAL REVIEW B VOLUME 24, NUMBER 6 15 SEPTEMBER 1981

Computer simulation of the radiation of axially channeled electrons

Y. Yamamura and Y. H. Ohtsuki*
Department of Applied Physics, Okayama University of Science, Ridai-cho, Okayama 700, Japan
(Received 29 April 1981)

Based on classical electrodynamics and the binary-collision approximation, the radiation emitted by axially channeled electrons has been investigated by computer simulation. It is found that the profiles of the photon spectra depend on whether or not the root-mean-square angle, $\langle\theta^2\rangle^{1/2}$ of emission of radiation is larger than the critical angle of the axial channeling. In the case that the root-mean-square angle is larger than the critical angle, the spectral peak of the radiation spectrum is very broad because of the contribution of dechanneled electrons. Especially under special conditions, there is the possibility that one can observe at very low energy the spectral peak which comes from the synchrotron radiation of dechanneled electrons. Comparison between the present simulated results and experimental results has revealed that the classical simulation can predict well the characteristic profile of the radiation of axially channeled electrons.

I. INTRODUCTION

The theory of bremsstrahlung of a relativistic particle moving in a crystal, which is well known as the Überall effect,[1] does not hold when the particle moves in the crystal under the channeling condition. Recently, Kumakov[2,3] has pointed out the possibility of spontaneous radiation of γ quanta by relativistic channeling leptons. This new physical effect was predicted to arise from transitions between the energetic levels of bound states formed in the field of atomic rows and planes.

This channeling radiation has been observed successfully by several authors. Alguard *et al.*[4–6] have measured the radiation from 56- and 28-MeV electrons and positrons which channel along the major axis or between major planes of a 18-μm-thick silicon crystal. For planar channeling, the observed photon spectra were found to have several spectral peaks in good agreement with the values evaluated as spontaneous transitions of energetic levels. For axial channeling, the observed spectra showed a large low-energy enhancement, which crested in the range from 100 to 300 keV.

Kalinin *et al.*[7] and Adishchev *et al.*[8] have measured the radiation emitted from axially channeled electrons with higher energies of incidence in a 0.3-mm-thick diamond crystal. Their measured photon spectra had a spectral peak with a long tail. They also showed that the variation of the peak energy ω_0 with energy of incidence can be well described as $\omega_0(E) = aE^{3/2}$, where a is an energy-independent constant.

In our previous paper,[9] we studied the radiation of axially channeled electrons by computer simulation, based on the binary-collision approximation and classical electrodynamics, where an electron trajectory is regarded as the superposition of instantaneous circular motions. In this paper, we calculated the photon spectrum of channeling radiation by Fourier transform of the electron trajectory in the three-dimensional crystal which is determined by the binary-collision approximation. It is already known that the axially channeled electron with a proper angular momentum performs a beautiful rosette motion along the major axis in the case where the effect of thermal vibration is small.[10] At a finite temperature, on the other hand, an electron trajectory shows a complicated spiral motion and such a complicated motion yields several spectral peaks. The correspondence of an electron trajectory and its associated photon spectrum is shown clearly in this paper.

The contribution of dechanneled electrons to the forward-emitted photon spectrum is also discussed. In cases where the root-mean-square (rms) angle of emission of radiation is larger than the critical angle of axial channeling, the dechanneled electrons con-

tribute largely to the photon emission spectrum and produce the featureless spectral structure with the low-energy enhancement such as the photon spectrum measured by Alguard *et al.*[5] In contrast, when the rms angle becomes comparable to the critical angle, the contribution of dechanneled electrons can be neglected and the forward-emitted photon spectrum is caused by the channeling radiation. The photon spectra measured by Adishchev *et al.*[8] correspond to this case.

The computation model was discussed in detail in Ref. 9. The effect of the thermal vibration and the beam divergence is included. In the present calculations, the contribution of ordinary bremsstrahlung can be estimated in a natural way.

II. GENERAL EXPRESSION FOR THE INTENSITY OF THE RADIATION

In the ultrarelativistic limits, the classical and quantum approaches yield close results, especially for axially channeled electrons.[2] The general form of the energy of the radiation from a relativistic particle per unit frequency and per unit solid angle is given in the classical electrodynamics by the formula[11]

$$\frac{d^2E}{d\omega d\Omega}=2\,|\,\vec{A}(\omega)\,|^2\,, \tag{1}$$

where $\vec{A}(\omega)$ is the Fourier component of the vector potential $\vec{A}(t)$ and is given by

$$A(\omega)=\left[\frac{e^2}{8\pi^2 c}\right]^{1/2}\int_{-\infty}^{\infty} e^{i\omega[t-\vec{n}\cdot\vec{r}(t)/c]}\frac{\vec{n}\times[(\vec{n}-\vec{\beta})\times\partial\vec{\beta}/\partial t]}{(1-\vec{n}\cdot\vec{\beta})^2}dt\,. \tag{2}$$

Here, $\vec{n}$ is a unit vector in the direction of the emitted γ photon $\vec{\beta}=\vec{v}/c$, $\vec{v}$ is the velocity, and $\vec{r}(t)$ is specified by the electron trajectory. Once $\vec{r}(t)$ is known for a specified motion, the vectors $\vec{\beta}(t)$ and $\partial\vec{\beta}(t)/\partial t$ can be determined. Then, the integral can be evaluated as a function of ω and the direction of $\vec{n}$. From the viewpoint of numerical calculation, it is very difficult to calculate the derivative $\partial\vec{\beta}(t)/\partial t$ numerically with small numerical errors. In order to minimize numerical errors, we used the following formula, which does not include the term $\partial\vec{\beta}(t)/\partial t$ and which is obtained by integrating Eq. (2) by parts.

$$\frac{d^2E}{d\omega d\Omega}=\frac{e^2\omega^2}{4\pi^2 c}\left|\int_{-\infty}^{\infty}\vec{n}\times(\vec{n}\times\vec{\beta})e^{i\omega[t-\vec{n}\cdot\vec{r}(t)/c]}dt\right|^2. \tag{3}$$

In the present calculations this simple formula is numerically evaluated after the electron trajectory is determined by the binary-collision approximation, where the Molière potential is employed for the calculation of the scattering angle. Since formula (2) can predict the photon spectrum emitted by ordinary bremsstrahlung and coherent bremsstrahlung, the present simulation can include the contributions of these well-known bremsstrahlung within the framework of the classical approximation.

III. NUMERICAL RESULTS AND DISCUSSIONS

Using the classical binary-collision approximation[12] and classical electrodynamics, we calculated the photon spectra emitted by relativistic electrons moving in the crystal along a major axis. In the present calculations, the ⟨110⟩ axis was employed as a major axis. The electrons are impinged onto the 1-μm-thick crystal (see Fig. 1), which is thinner than the crystals used in the experiments. The angular divergence and the energy spread of the electron beam are set to be equal to the experimental conditions.

Before discussing the numerical results, let us obtain a well-known formula for the photon spectrum emitted by a single electron trajectory. In the energy range of interest, it can be assumed that the velocity $\vec{v}(t)$ is equal to the electron velocity of incidence $\vec{v}$ and that only the perpendicular component of $\vec{\beta}(t)$ to the velocity $\vec{v}$ is a function of time. Furthermore, the rms angle $\langle\theta^2\rangle^{1/2}\simeq 1/\gamma$ of the photon beam is larger than the critical angle of the axial channeling, where γ is the relativistic fac-

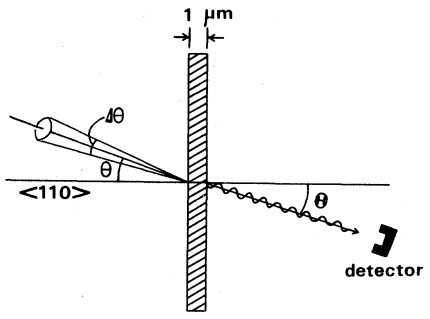

FIG. 1. Geometry of channeling radiation.

tor. This means that the forward-directed radiation comes from the overall channeling trajectory. Substituting Eq. (2) into Eq. (1) and integrating Eq. (1) with respect to the solid angle yields[13,14]

$$\frac{dE}{d\omega}=\frac{N_c e^2}{T_c c^3}\sum_{g_n>\delta}\frac{\omega W_T^2(g_n)}{g_n^2}\left[1-2\frac{\delta}{g_n}\left[1-\frac{\delta}{g_n}\right]\right], \tag{4}$$

where it is assumed that the trajectory of an electron deviated periodically for the original direction. Here, T_c is the period of the oscillation, N_c is the number of cycles, and

$$W_T(g_n)=\int_0^T dt\,\beta(t)e^{ig_n t}, \tag{5}$$

$$\delta=\omega/2\gamma^2,\quad g_n=2\pi n/T_c\ .$$

The main term of Eq. (4) is equal to Kumakov's radiation formula and has the spectral peak at $\omega=\omega_0$, where $\omega_0=2\gamma^2 g_0$.

Figure 2 shows electron trajectories in the transverse plane to the ⟨110⟩ axis and the associated photon spectra, where 56-MeV electrons are impinged on the silicon crystal and the thermal vibration is ignored. The trajectory of Fig. 2(a) is the case with large angular momentum and this electron is trapped in two adjacent major axes. In the case of medium angular momentum, which is shown in Fig. 2(b), the channeling electron is well trapped in the effective potential valley and performs a typical rosette motion.[10] The photon spectrum emitted by this rosette motion has sharp peaks at higher energies. The case of small angular momentum is shown in Figs. 2(c) and 2(d). In this case, an electron is significantly scattered at the atom in the row, because an electron with small angular momentum can approach the critical spiral distance.

The spectrum of Fig. 2(c) has a smooth peak at very low energy, which may be due to the emission from the dechanneled trajectory. As is shown in Table I, the rms angle of the photon beam is larger than the critical angle, and so a dechanneled elec-

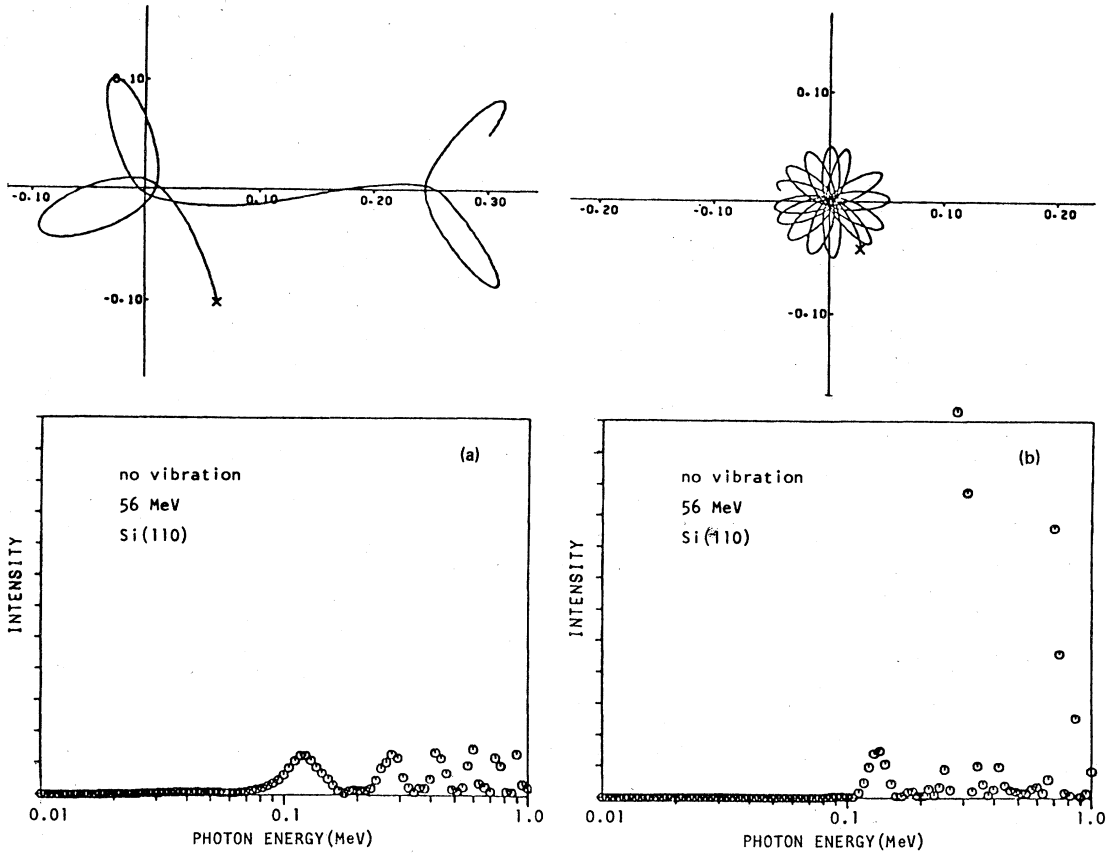

FIG. 2. Electron trajectories in the transverse plane and the associated photon intensity spectra, where the thermal vibration is ignored.

TABLE I. The root-mean-square angles of emission of radiation and the critical angles of the axial channeling for different energies of incidence.

Incident energy (MeV)	Target	Root-mean-square angle $\langle\theta^2\rangle^{1/2}$	Critical angle of $\langle 110\rangle$ axial channeling ψ_c	Ratio $\eta=\langle\theta^2\rangle^{1/2}/\psi_c$
56	silicon (110)	0.52°	0.078°	6.6
600	diamond (110)	0.049°	0.019°	2.5
750	diamond (110)	0.039°	0.017°	2.3
900	diamond (110)	0.033°	0.016°	2.0

tron can contribute to the photon intensity observed at $\Theta=0°$. In other words, this low-energy peaking is a kind of a synchrotron radiation which has the peak at $\omega\simeq\gamma^3(c/\rho)$, where ρ is the radius of curvature. The radius of the instantaneous circular motion corresponding to this peak value is of the order of 10^{-3} cm.

Figure 3 shows the trajectories and the corresponding spectra at a finite temperature ($T=300$ K). These trajectories are appreciably different from those in Fig. 2. The trapped electrons show a complicated motion along the axis. Figure 3(d) shows a very interesting trajectory, which includes two types of spiral motions. The rosettelike motion around the adjacent axis produces the spectral peak at the lower energy.

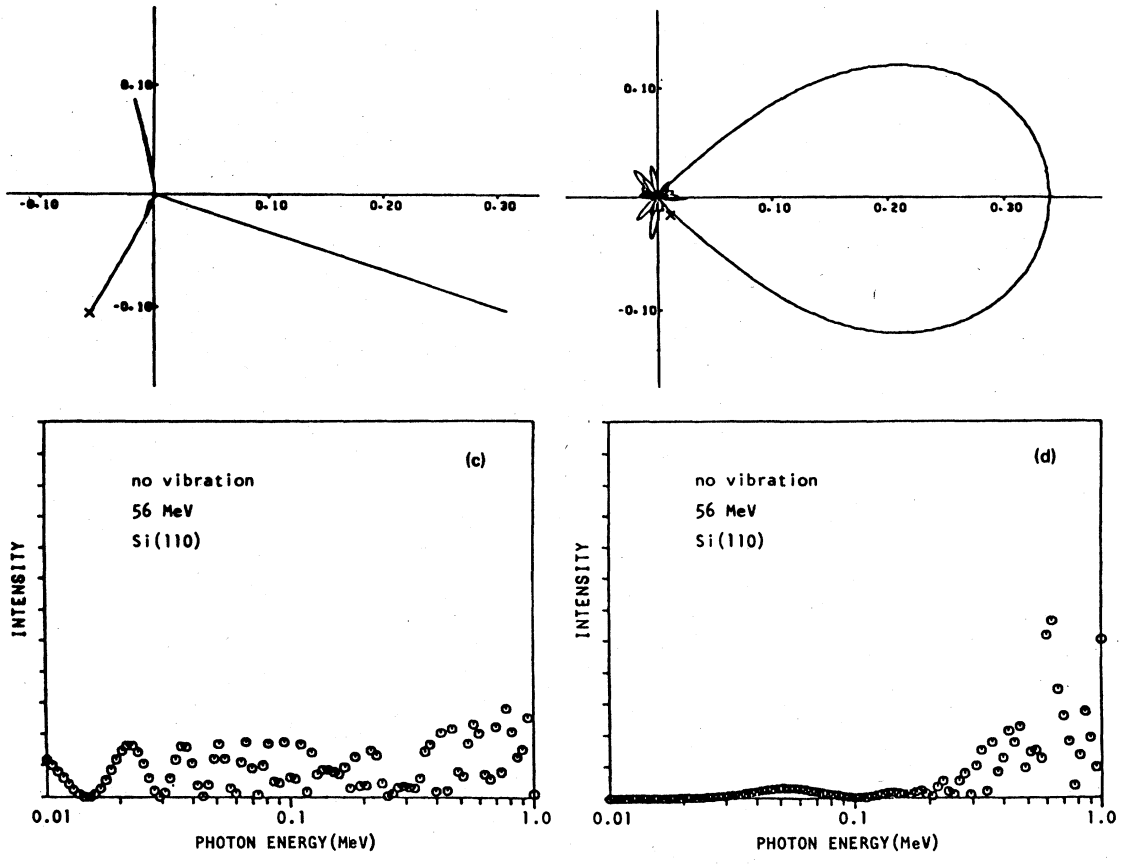

FIG. 2. *(Continued.)*

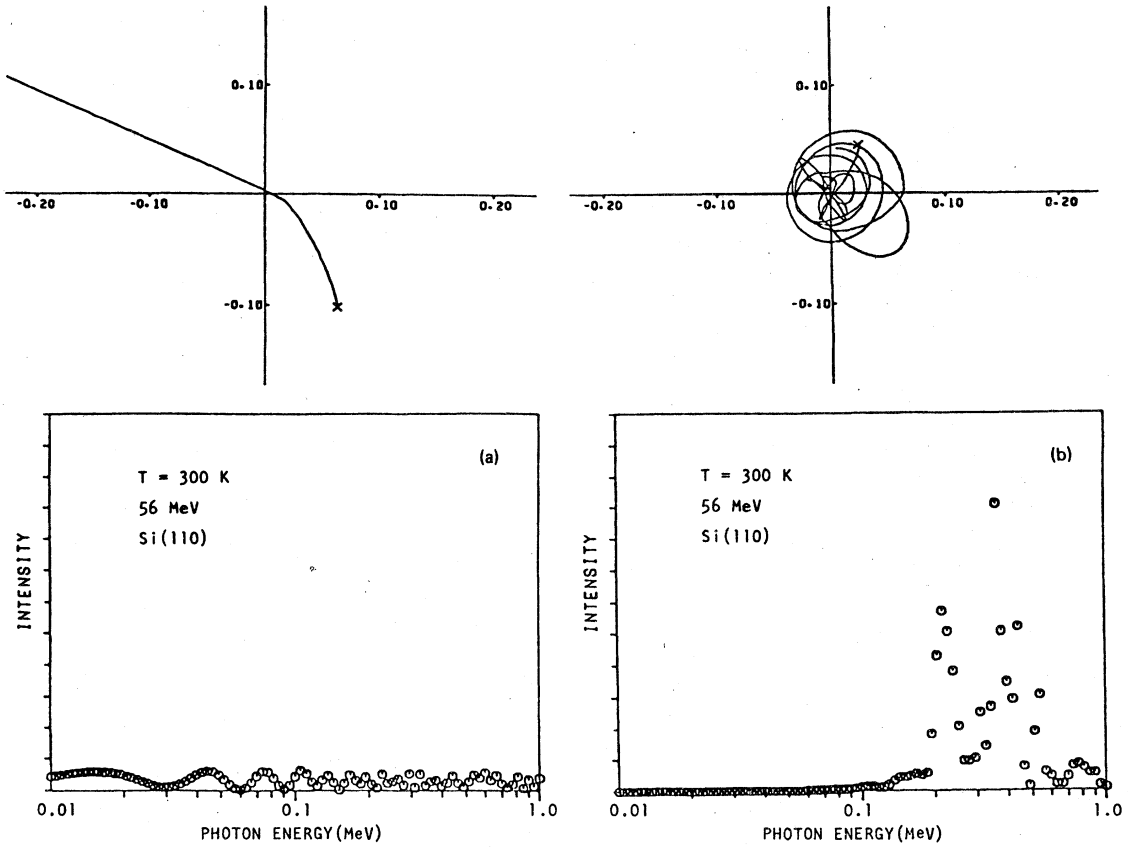

FIG. 3. Electron trajectories in the transverse plane and associated photon intensity spectra at $T=300$ K.

The photon emission spectra averaged over many trajectories are plotted in Fig. 4. The open circles indicate the total intensity under the condition of $\theta=0°$, $\Delta\theta=0.114°$, and $\Theta=0°$, and the solid circles correspond to the "random" spectrum, which is simulated by changing the azimuthal angle and the polar angle of incidence randomly. The solid triangles denote the radiation emitted by axially channeled electrons, i.e., $\hat{\theta}<\psi_c$, where $\hat{\theta}=\cos^{-1}[\vec{n}\cdot\vec{r}(t)]$. Since the rms angle is larger than the axial critical angle (see Table I), the forward-directed radiation is composed of the channeling part and the random part, which are comparable in the present calculation. Swent's experimental result suggested that the ratio of the channeling emission spectrum to the random spectrum was about 8 on the average. This discrepancy may be due mainly to the difference of thickness of the employed crystal. For the thick crystal, the number of cycles N_c is on the average larger than that of the thin crystal. As is known from Eq. (4), the larger N_c emits the channeling radiation with the higher intensity. On the other hand, dechanneled electrons are more randomly oriented for the thicker crystal. This may reduce relatively the intensity of the random spectrum. However, it is very difficult to explain the large experimental ratio within the framework of the present calculations. One must investigate further the contribution of the angular divergence of the incident beam, the temperature, and the interaction potential to the intensity of the channeling radiation.

The comparison between the calculated spectrum and the experimental result is shown in Fig. 5, where the intensity is normalized at the peak. The open and solid circles indicate the present simulated result and the experimental spectrum, respectively. With regard to the overall profile, agreement is good, but the maximal radiation energy of our result is larger by about 50 keV than the experimental one. The calculated spectrum has the peak at the low energy, which is not observed in the experimental spectrum. This peaking is the contribution of dechanneled electrons, which is known from

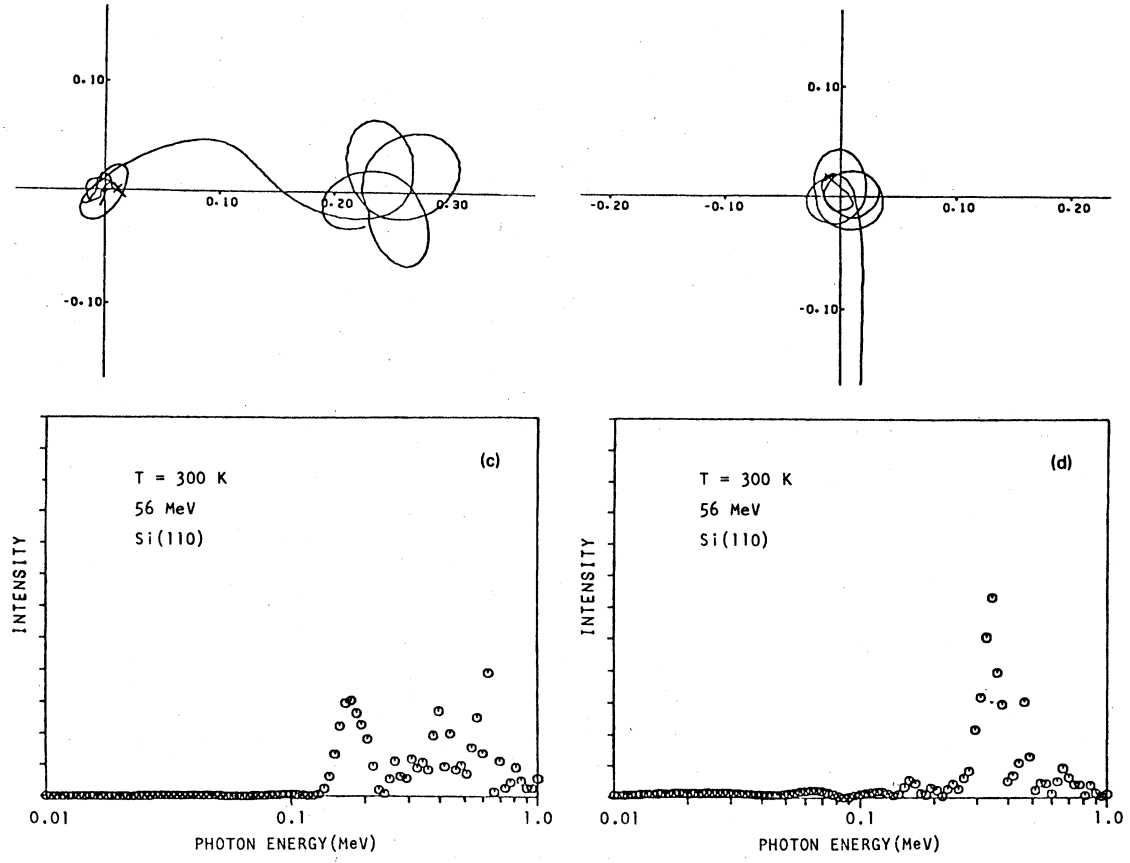

FIG. 3. *(Continued.)*

comparison between the solid circle spectrum and the triangle spectrum in Fig. 4. The dechanneled electrons, which can contribute the intensity observed at $\Theta=0°$, must have the limited polar angle against the axis, i.e., $\psi_c < \hat{\theta} < \langle \theta^2 \rangle^{1/2}$. Since the instantaneous circular motion with small radius does not occur often because of small cross section, the available dechanneled electrons move at constant speeds on the circular path with similar radii of curvature. Moreover, the crystal employed for the present simulation is not thick enough for directions

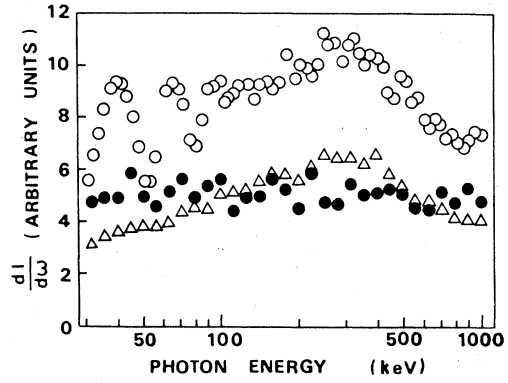

FIG. 4. Photon intensity spectra of channeling radiation for 56-MeV electrons impinged onto the (110) face of a silicon crystal.

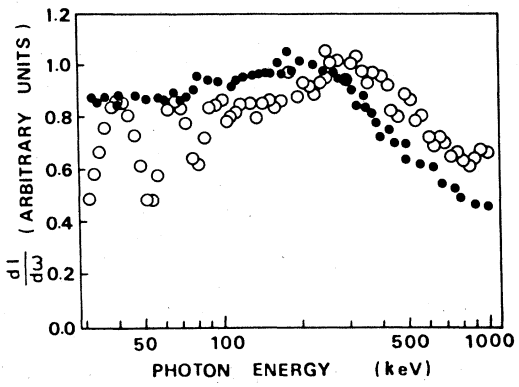

FIG. 5. Comparison of the calculated spectrum with the experimental spectrum. ○○○ the present calculated spectrum; ●●● the experimental spectrum (Ref. 5).

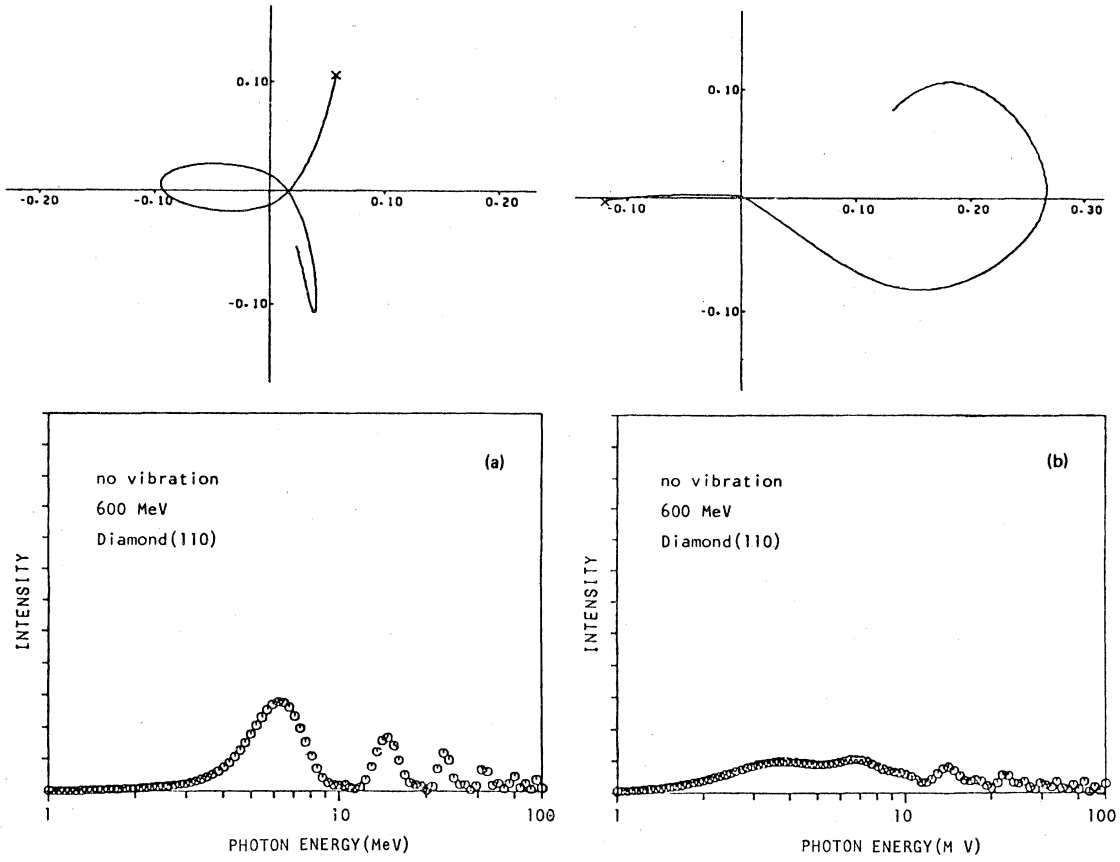

FIG. 6. Electron trajectories and the associated photon intensity spectra, where the thermal vibration is ignored.

of dechanneled electrons to be completely random. This means that under special conditions the photon spectrum has the spectral peak at very low energy which comes from the synchrotron radiation of dechanneled electrons.

Figures 6 and 7 correspond to Figs. 2 and 3, respectively, where a 600-MeV electron is impinged onto the (110) face of a diamond crystal under the conditions of $\theta=0°$ and $\Theta=0°$. Since the ratio η is small as compared with the case of a 56-MeV electron on the silicon crystal (see Table I), the radiation from the dechanneled electron does not influence as much the intensity observed at $\Theta=0°$. This can be known from the comparison of Fig. 6(d) with Fig. 2(c).

Figures 8, 9, and 10 show the calculated intensity spectra for channeling electrons with energies $E=600$, 750, and 900 MeV, respectively, where Adishchev's experimental results are also plotted by solid circles. The lower squares in these figures represent the random spectrum, which is calculated under the conditions of $\theta=3°$ and $\Delta\theta=0.0172°$, while open circles correspond to the total photon intensity of channeling radiation simulated under the conditions of $\theta=0°$, $\Delta\theta=0.0172°$, and $\Theta=0°$. As a whole, agreements are very good, especially the simulated spectrum of 600-MeV energy that has the shoulder peak of the experimental result, which appears at an energy slightly larger than the maximal radiation energy ω_0. In the present calculations the ratios of the peak intensities to those of the random part are 4.2, 3.8, and 3.5, respectively, for 600-, 750-, and 900-MeV energies of incidence. These values are smaller than the experimental results, which are about 7 for these three energies of incidence. This discrepancy is due to the difference of the crystal thickness, which is easily realized if one compares the trajectories in Fig. 2 with those in Fig. 6.

The angular distributions of emitted photons are also plotted in Fig. 11, where the experimental results are described by the broken lines. Agree-

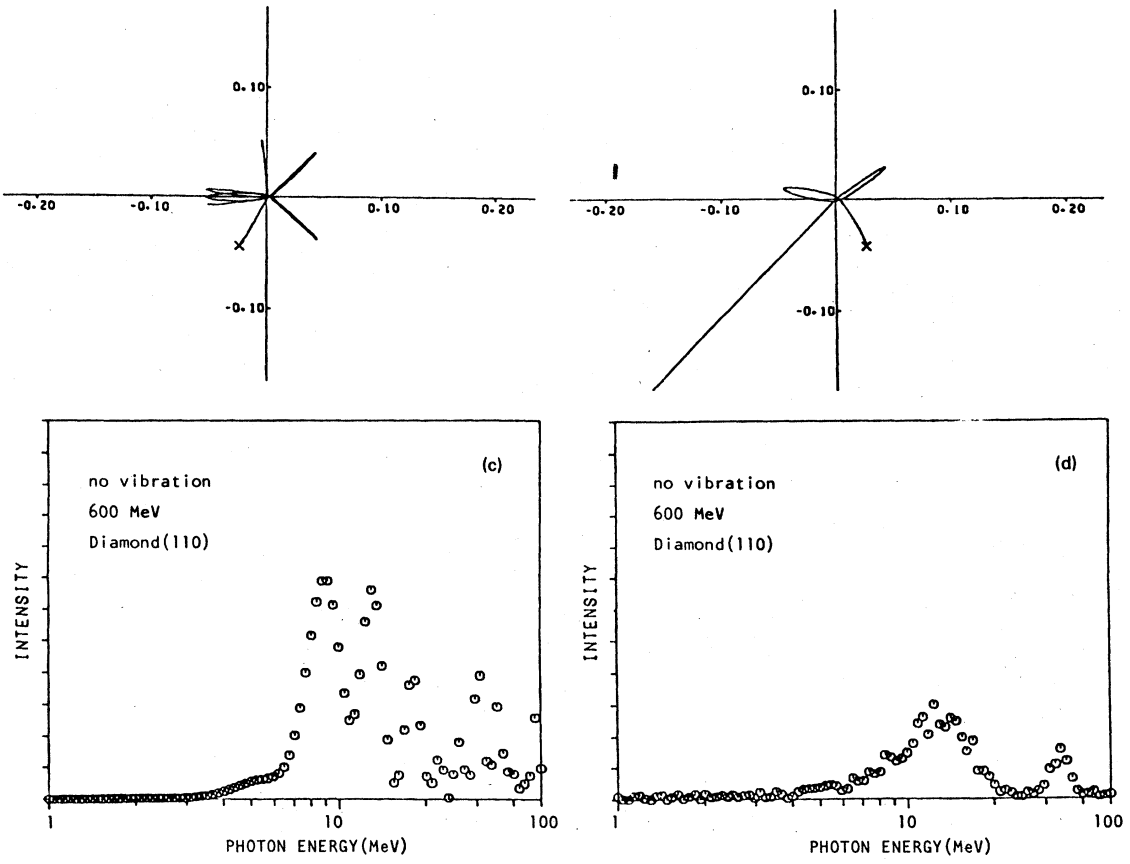

FIG. 6. *(Continued.)*

ment between the simulated results and Adishchev's experimental results is very good. The calculated distributions have the fine structure. According to classical electrodynamics, in the ultrarelativistic limits, the angle for which the intensity is a maximum is given by $\theta_{max}=1/2\gamma$. For 900-MeV energy of incidence, the maximal angle is 0.28 mrad, which agrees with the peak values of our calculated distributions. It is reasonable that the peak does not appear in the experimental distributions, because the angular acceptance of their detector is larger than the angle θ_{max}.

TABLE II. Comparison of our calculated maximal radiation energies and boundary energies with the experimental results.

Incident energy E (MeV)	Experimental value or calculated value	Maximal radiation energy ω_0 (MeV)	Boundary energy ω_{max} (MeV)
600	Expt.	9 ± 1	60 ± 5
	Calc.	7	60 ± 10
750	Expt.	13 ± 1	95 ± 5
	Calc.	10	90 ± 10
900	Expt.	17 ± 1	130 ± 5
	Calc.	13	120 ± 10

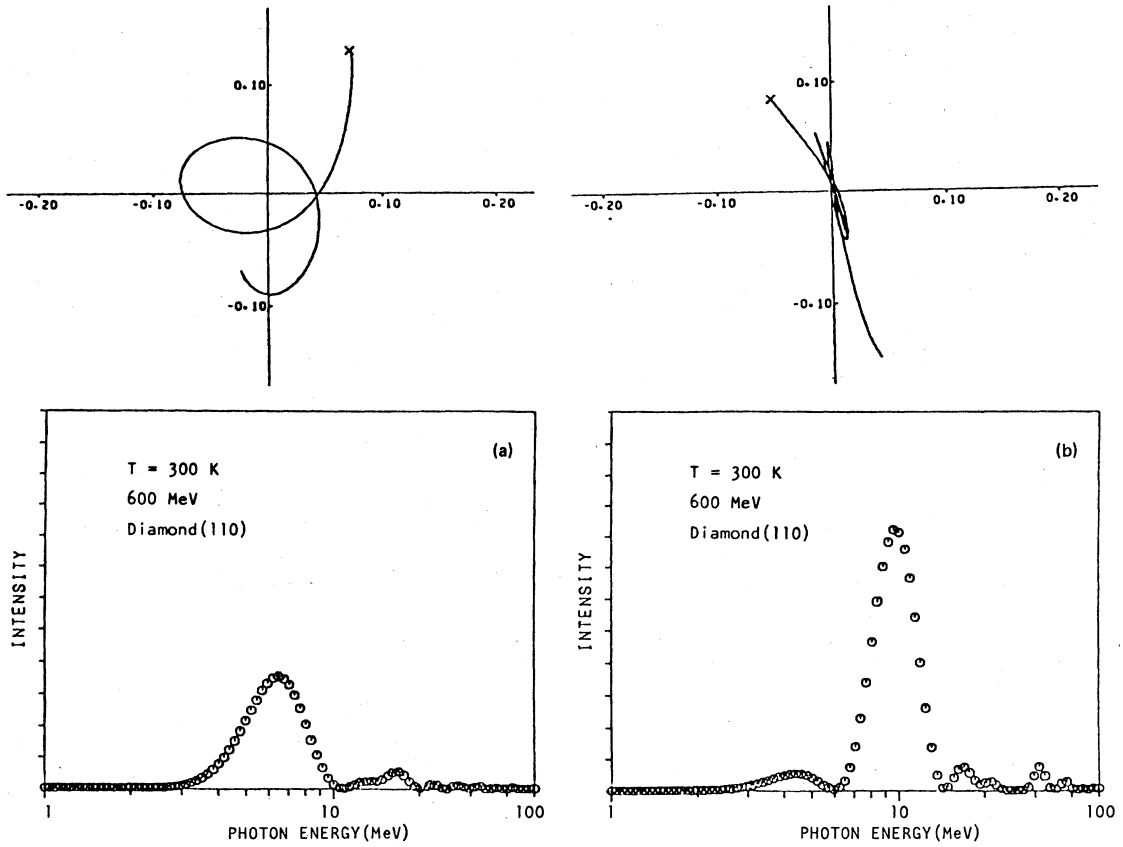

FIG. 7. Electron trajectories and the associated photon intensity spectra at $T=300$ K.

The maximal radiation energy ω_0 and the boundary energy ω_{max} are listed in Table II. The calculated values are in good agreement with Adishchev's experimental results, though our maximum energies are slightly lower than the experimental values. Our maximal radiation energy ω_0 is also described as $\omega_0(E)=aE^{3/2}$. As is known from Figs. 6 and 7, the spiral trajectories will be stable at $r_c < r < r_0$, where r is the spiral radius, r_c is the critical distance, and r_0 is half the distance between two neighboring atomic rows. This gives the boundary energy ω_{max} of the spectral region of channeling radiation, i.e., $\omega_{max}=2\gamma^2\hat{\theta}_{max}/r_c$. If one sets $\hat{\theta}_{max}=\psi_c$ and r_c is equal to the Thomas-Fermi screening length, this rough estimation yields 55, 79, and 105 MeV as ω_{max} for 600-, 750-, and 900-MeV energies of incidence, respectively.

IV. CONCLUSIONS

Based on the classical binary-collision approximation and classical electrodynamics, the forward-directed radiation from axially channeled electrons has been investigated and the computational results are compared with data from two recent experiments. As a whole, agreements between the present calculated results and the experimental results are very good.

In the case of the relatively low energy of incidence where the root-mean-square angle of emission of radiation is larger than the critical angle of the axial channeling, the radiation from dechanneled electrons is very important. The calculated photon spectrum has another spectral peak at very low energy, which does not appear in the experimental

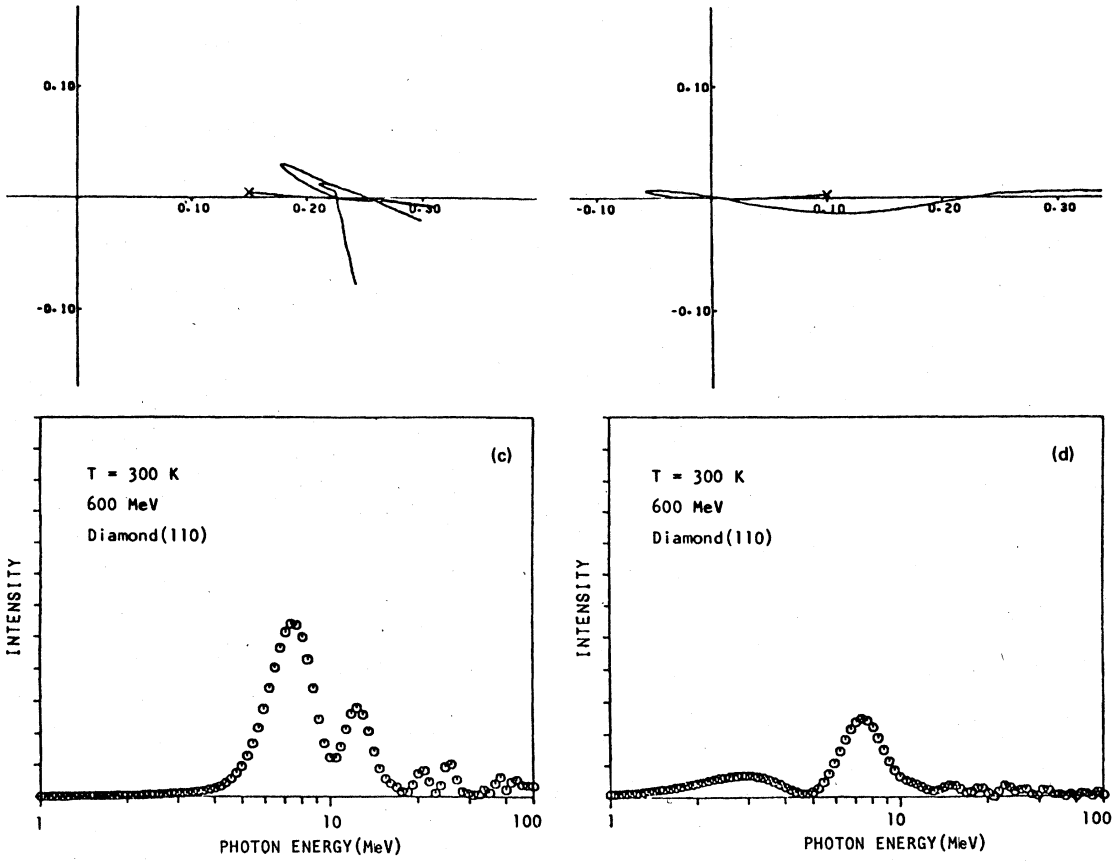

FIG. 7. *(Continued.)*

spectrum[15] The maximal radiation energy of the former spectrum is lower than the experimental value, but the overall profile of the intensity spectrum is in good agreement with that of the experimental one.

In the case of the high energy of incidence where

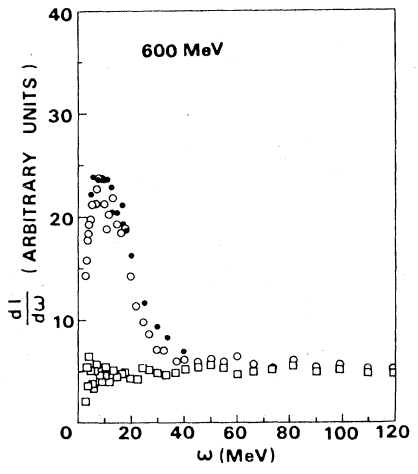

FIG. 8. Photon intensity spectra of channeling radiation for 600-MeV electrons.

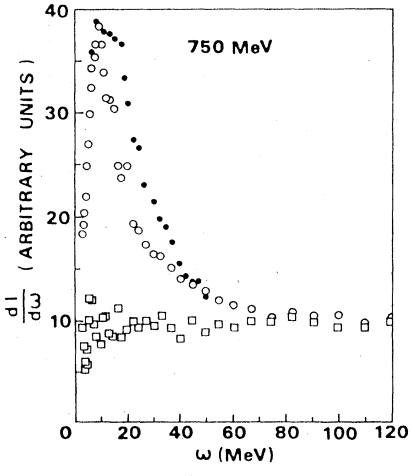

FIG. 9. Photon intensity spectra of channeling radiation for 750-MeV electrons.

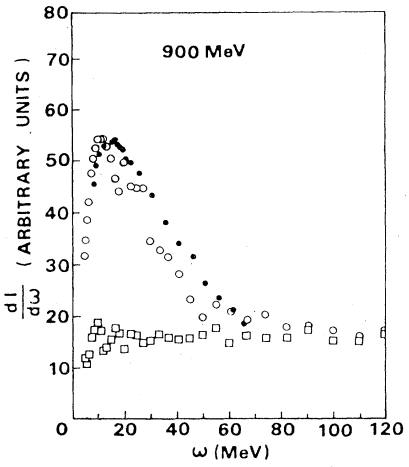

FIG. 10. Photon intensity spectra of channeling radiation for 900-MeV electrons.

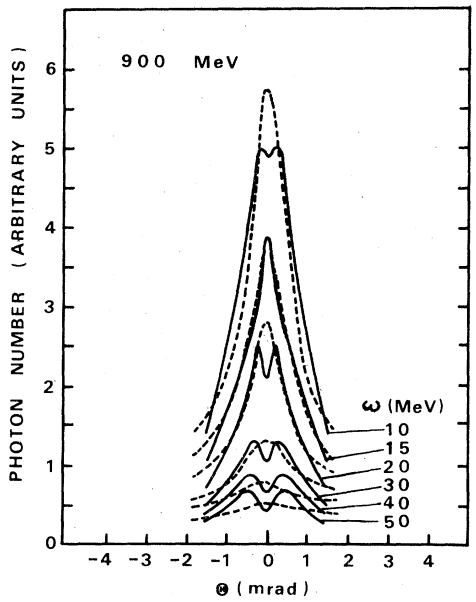

FIG. 11. Angular distributions of the yield of photon with different energies for 900-MeV electrons impinged along the ⟨110⟩ axis of diamond, where the experimental profiles and the simulated profiles are normalized at the peak of the angular distributions of $\omega = 15$ MeV.

the root-mean-square angle of the photon beam is comparable to the critical angle, the forward-directed radiation is mainly composed of the channeling radiation and agreement between calculated spectra and experimental ones[8] is very good. In this case the radiation from dechanneled electrons does not influence as much the profile of the intensity spectrum observed at the direction of the incident electron beam.

From comparison between the simulated results and the experimental ones it is found that the classical binary-collision approximation and the classical electrodynamical approach can predict well the characteristics of the axial channeling radiation. However, one must investigate further the contribution of the angular divergence and the temperature to the forward-directed radiation.

*Department of Physics, Waseda University, Ohkubo, Shinjuku-ku, Tokyo 160, Japan.

[1]H. Uberall, Phys. Rev. 103, 1055 (1956).
[2]M. A. Kumakov, Phys. Lett. 57A, 17 (1976).
[3]M. A. Kumakov, Zh. Eksp. Teor. Fiz. 72, 1489 (1977) [Sov. Phys.—JETP 45, 781 (1977)].
[4]M. J. Alguard, R. L. Swent, R. H. Pantell, B. L. Berman, S. D. Bloom, and S. Datz, Phys. Rev. Lett. 30, 265 (1979).
[5]R. L. Swent, R. H. Pantell, M. J. Alguard, B. L. Berman, S. D. Bloom, and S. Datz, Phys. Rev. Lett. 43, 1723 (1979).
[6]M. J. Alguard, R. L. Swent, R. H. Pantell, S. Datz, J. H. Barrett, B. L. Berman, and S. D. Bloom, Nucl. Instrum. Methods 170, 7 (1980).
[7]B. N. Kalinin, V. V. Kaplin, A. P. Potalitsin, and S. A. Vorobiev, Phys. Lett. 70A, 447 (1979).
[8]Y. N. Adishchev, V. V. Kaplin, A. P. Potalitsin, and S. A. Vorobiev, Phys. Lett. 75A, 316 (1980).
[9]Y. Yamamura and Y. H. Ohtsuki, Radiat. Eff. (in press).
[10]H. Kumm, F. Bell, R. Sizmann, H. J. Kreiner, and D. Harder, Radiat. Eff. 12, 53 (1972).
[11]J. D. Jackson, Classical Electrodynamics (Wiley, New York, 1975).
[12]Y. Yamamura and W. Takeuchi, Radiat. Eff. 42, 55 (1979).
[13]A. I. Akhiezer, Z. A. Akhiezer, and N. F. Shul'ga, Zh. Eksp. Teor. Fiz 76, 1244 (1979) [Sov. Phys.—JETP 49, 631 (1979)].
[14]L. D. Landau and E. M. Lifshitz, *Field Theory* (Pergamon, Oxford, 1975).